

# Waveguide saturable absorbers at 1.55 $\mu\text{m}$ based on intraband transitions in GaN/AlN QDs

L. Monteagudo-Lerma,<sup>1,6,\*</sup> S. Valdueza-Felip,<sup>2,6</sup> F. B. Naranjo,<sup>1</sup> P. Corredera,<sup>3</sup> L. Rapenne,<sup>4</sup> E. Sarigiannidou,<sup>4</sup> G. Strasser,<sup>5</sup> E. Monroy,<sup>2</sup> and M. González-Herráez<sup>1</sup>

<sup>1</sup> GRIFO, Dpto. Electrónica, Universidad de Alcalá, Madrid-Barcelona km 33.6, 28871 Alcalá de Henares, Spain

<sup>2</sup> CEA-Grenoble, INAC/SP2M, 17 rue des Martyrs, 38054 Grenoble, France

<sup>3</sup> Instituto de Óptica, CSIC, Serrano 121, 28006 Madrid, Spain

<sup>4</sup> INP-Grenoble/Minatoc, 3 parvis Louis Néel BP257, 38016 Grenoble, France

<sup>5</sup> Zentrum für Mikro- und Nanostrukt., TU Vienna, Floragasse 7, 1040 Vienna, Austria

<sup>6</sup> These author contributed equally to the authorship of this paper.

\*[laura.monteagudo@depeca.uah.es](mailto:laura.monteagudo@depeca.uah.es)

**Abstract:** We report on the design, fabrication and optical characterization of GaN/AlN quantum-dot-based waveguides for all-optical switching via intraband absorption saturation at 1.55  $\mu\text{m}$ . The transmittance of the TM-polarized light increases with the incident optical power due to the saturation of the  $s$ - $p_z$  intraband absorption in the QDs. Single-mode waveguides with a ridge width of 2  $\mu\text{m}$  and a length of 1.5 mm display 10 dB absorption saturation of the TM-polarized light for an input pulse energy of 8 pJ and 150 fs.

©2013 Optical Society of America

**OCIS codes:** (190.5970) Semiconductor nonlinear optics including MQW; (230.7370) Waveguides; (230.1150) All-optical devices.

## References and links

- O. Wada, "Femtosecond all-optical devices for ultrafast communication and signal processing," *New J. Phys.* **6**, 183 (2004).
- V. R. Almeida, C. A. Barrios, R. R. Panepucci, and M. Lipson, "All-optical control of light on a silicon chip," *Nature* **431**(7012), 1081–1084 (2004).
- N. Bloembergen, "Nonlinear optics: past, present, and future," *IEEE J. Sel. Top. Quant.* **6**(6), 876–880 (2000).
- K. S. Kim, R. H. Stolen, W. A. Reed, and K. W. Quoi, "Measurement of the nonlinear index of silica-core and dispersion-shifted fibers," *Opt. Lett.* **19**(4), 257–259 (1994).
- C. Vinegoni, M. Wegmuller, and N. Gisin, "Measurements of the nonlinear coefficient of standard SMF, DSF, and DCF fibers using a self-aligned interferometer and a Faraday mirror," *IEEE Photonic Tech. L.* **13**(12), 1337–1339 (2001).
- M. González-Herráez, *Advanced Fibre Optics: Concepts and Technology* (EPFL Press, 2011).
- R. W. Boyd, *Nonlinear Optics*, 3rd edn (Academic Press, 2008).
- S. Radic and C. J. Mc Kinstrie, "Optical amplification and signal processing in highly nonlinear optical fiber," *IEICE Trans. Electron.* **E88-C**(5), 859–869 (2005).
- S. Noda, T. Yamashita, M. Ohya, Y. Muromoto, and A. Sasaki, "All-optical modulation for semiconductor lasers by using three energy levels in n-doped quantum wells," *IEEE J. Quantum Electron.* **29**(6), 1640–1647 (1993).
- H. Morkoç, *Handbook of Nitride Semiconductors and Devices*, Vol. 2 (Wiley-VCH, 2008).
- F. B. Naranjo, M. González-Herráez, H. Fernández, J. Solís, and E. Monroy, "Third order nonlinear susceptibility of InN at near band-gap wavelengths," *Appl. Phys. Lett.* **90**(9), 091903 (2007).
- F. B. Naranjo, P. K. Kandaswamy, S. Valdueza-Felip, V. Calvo, M. González-Herráez, S. Martín-López, P. Corredera, J. A. Méndez, G. R. Mutta, B. Lacroix, P. Ruterana, and E. Monroy, "Nonlinear absorption of InN/InGaN multiple-quantum-well structures at optical telecommunication wavelengths," *Appl. Phys. Lett.* **98**(3), 031902 (2011).
- S. Valdueza-Felip, L. Rigutti, F. B. Naranjo, P. Ruterana, J. Mangeney, F. H. Julien, M. González-Herráez, and E. Monroy, "Carrier localization in InN/InGaN multiple-quantum wells with high In-content," *Appl. Phys. Lett.* **101**(6), 062109 (2012).
- M. Beeler, E. Trichas, and E. Monroy, "III-nitride semiconductors for intersubband optoelectronics: a review," *Semicond. Sci. Technol.* **28**(7), 074022 (2013).
- M. Tcherysheva, L. Nevou, L. Doyennette, F. H. Julien, E. Warde, F. Guillot, E. Monroy, E. Bellet-Amalric, T. Remmele, and M. Albrecht, "Systematic experimental and theoretical investigation of intersubband absorption in GaN/AlN quantum wells," *Phys. Rev. B* **73**(12), 125347 (2006).

16. J. Hamazaki, S. Matsui, H. Kunugita, K. Ema, H. Kanazawa, T. Tachibana, A. Kikuchi, and K. Kishino, "Ultrafast intersubband relaxation and nonlinear susceptibility at 1.55  $\mu\text{m}$  in GaN/AlN multiple-quantum wells," *Appl. Phys. Lett.* **84**(7), 1102 (2004).
17. J. D. Heber, C. Gmachl, H. M. Ng, and A. Y. Cho, "Comparative study of ultrafast intersubband electron scattering times at  $\sim 1.55$   $\mu\text{m}$  wavelength in GaN/AlGaIn heterostructures," *Appl. Phys. Lett.* **81**(7), 1237 (2002).
18. N. Suzuki and N. Iizuka, "Feasibility study on ultrafast nonlinear optical properties of 1.55- $\mu\text{m}$  intersubband transition in AlGaIn/GaN Quantum Wells," *Jpn. J. Appl. Phys.* **36**(Part 2, No. 8A), L1006–L1008 (1997).
19. N. Iizuka, K. Kaneko, N. Suzuki, T. Asano, S. Noda, and O. Wada, "Ultrafast intersubband relaxation ( $< 150$  fs) in AlGaIn/GaN multiple quantum wells," *Appl. Phys. Lett.* **77**(5), 648–650 (2000).
20. R. Rapaport, G. Chen, O. Mitrofanov, C. Gmachl, H. M. Ng, and S. N. G. Chu, "Resonant optical nonlinearities from intersubband transitions in GaN/AlN quantum wells," *Appl. Phys. Lett.* **83**(2), 263–265 (2003).
21. S. Valdueza-Felip, F. B. Naranjo, M. González-Herráez, H. Fernández, J. Solís, F. Guillot, E. Monroy, L. Nevou, M. Tchernycheva, and F. H. Julien, "Characterization of the resonant third-order nonlinear susceptibility of Si-doped GaN/AlN quantum wells and quantum dots at 1.5  $\mu\text{m}$ ," *IEEE Photonic Tech. L.* **20**(16), 1366–1368 (2008).
22. L. Nevou, M. Tchernycheva, F. H. Julien, M. Raybaut, A. Godard, E. Rosencher, F. Guillot, and E. Monroy, "Intersubband resonant enhancement of second-harmonic generation in GaN/AlN quantum wells," *Appl. Phys. Lett.* **89**(15), 151101 (2006).
23. N. Suzuki, N. Iizuka, and K. Kaneko, "Intersubband transition in AlGaIn-GaN quantum wells for ultrafast all-optical switching at communication wavelength," *Proc. SPIE* **3940**, Ultrafast Phenomena in Semiconductors **IV**, 127 (2000).
24. Y. Li, A. Bhattacharyya, C. Thomidis, T. D. Moustakas, and R. Paiella, "Ultrafast all-optical switching with low saturation energy via intersubband transitions in GaN/AlN quantum-well waveguides," *Opt. Express* **15**(26), 17922–17927 (2007).
25. N. Iizuka, H. Yoshida, N. Managaki, T. Shimizu, S. Hassanet, C. Cumtornkittikul, M. Sugiyama, and Y. Nakano, "Integration of GaN/AlN all-optical switch with SiN/AlN waveguide utilizing spot-size conversion," *Opt. Express* **17**(25), 23247–23253 (2009).
26. L. Nevou, J. Mangeney, M. Tchernycheva, F. H. Julien, F. Guillot, and E. Monroy, "Ultrafast relaxation and optical saturation of intraband absorption of GaN/AlN quantum dots," *Appl. Phys. Lett.* **94**(13), 132104 (2009).
27. S. Birner, T. Zibold, T. Andlauer, T. Kubis, M. Sabathil, A. Trellakis, and P. Vogl, "nextano: General Purpose 3-D Simulations," *IEEE T. Electron Dev.* **54**(9), 2137–2142 (2007).
28. P. K. Kandaswamy, F. Guillot, E. Bellet-Amalric, E. Monroy, L. Nevou, M. Tchernycheva, A. Michon, F. H. Julien, E. Baumann, F. R. Giorgetta, D. Hofstetter, T. Remmele, M. Albrecht, S. Birner, and L. S. Dang, "GaN/AlN short-period superlattices for intersubband optoelectronics: A systematic study of their epitaxial growth, design, and performance," *J. Appl. Phys.* **104**(9), 093501 (2008).
29. F. Guillot, E. Bellet-Amalric, E. Monroy, M. Tchernycheva, L. Nevou, L. Doyennette, F. H. Julien, L. S. Dang, T. Remmele, M. Albrecht, T. Shibata, and M. Tanaka, "Si-doped GaN/AlN quantum dot superlattices for optoelectronics at telecommunication wavelengths," *J. Appl. Phys.* **100**(4), 044326 (2006).
30. N. Gogneau, G. Jalabert, E. Monroy, E. Sarigiannidou, J.-L. Rouvière, T. Shibata, M. Tanaka, J.-M. Gérard, and B. Daudin, "Influence of AlN overgrowth on structural properties of GaN quantum wells and quantum dots grown by plasma-assisted molecular beam epitaxy," *J. Appl. Phys.* **96**(2), 1104–1110 (2004).
31. R. G. Hunsperger, *Integrated Optics: Theory and Technology*, 4th edn (Springer, 1995).
32. Y. Li, A. Bhattacharyya, C. Thomidis, T. D. Moustakas, and R. Paiella, "Nonlinear optical waveguides based on near-infrared intersubband transitions in GaN/AlN quantum wells," *Opt. Express* **15**(9), 5860–5865 (2007).
33. Y. Li, A. Bhattacharyya, C. Thomidis, Y. Liao, T. D. Moustakas, and R. Paiella, "Refractive-index nonlinearities of intersubband transitions in GaN/AlN quantum-well waveguides," *J. Appl. Phys.* **104**(8), 083101 (2008).

## 1. Introduction

The increasing bandwidth demand in optical communication networks based on multi-terabit wavelength and time division multiplexing impels the development of all-optical devices (switches, routers, wavelength converters), particularly targeting the C-band of optical fibers ( $\sim 1.55$   $\mu\text{m}$ ), where erbium-doped fiber amplifiers are widely available. All-optical switches should be capable of sustaining high repetition rates (subpicosecond response time) with low switching energy and high modulation depths, features that lead to consider the use of resonant nonlinearities [1]. Highly nonlinear fibers and waveguides (WG) have been used for generating nonlinear interactions in this spectral region [2,3]. However, due to the low values of their nonlinear coefficients ( $n_2$ :  $2.5 \times 10^{-16}$   $\text{cm}^2/\text{W}$  at 1.55  $\mu\text{m}$  in silica fibers [4,5]), the implementation of devices often requires long interaction distances (even kilometers in the case of nonlinear fibers) or high power levels [6], making them cumbersome for real systems.

An interesting alternative comes through the use of semiconductor third-order nonlinearities, exploiting phenomena like nonlinear absorption, self- and cross-phase

modulation, self- and cross-gain modulation, and four-wave mixing [7,8]. In this case, switching can be achieved through absorption saturation by an intense control pulse, as originally demonstrated at long infrared wavelengths using GaAs/AlGaAs structures [9]. From this point of view, III-nitride semiconductors are good candidates since the asymmetry of their crystalline structure contributes to enhance nonlinear phenomena [10]. There are two different approaches to cover the near-infrared spectral range using nitride semiconductors. A first strategy is the use of InN, which presents a room temperature direct bandgap of 0.64 eV (:1.94  $\mu\text{m}$ ). For this purpose, Naranjo *et al.* explored the potential of InN films and InN/InGaN multi-quantum-well structures with interband transitions at 1.55  $\mu\text{m}$ , by analyzing their third-order nonlinear susceptibility ( $\chi^{(3)}$ ) [11] and their nonlinear absorption [12]. For these structures, a minimum recovery time in the range of tens of ps can be achieved [13].

A second approach consists on using intra-conduction-band transitions in GaN/AlN nanostructures, namely the passage from the ground electronic state to the first excited state ( $e_1-e_2$ ) in quantum wells (QWs), or to the first state confined along the [0001] growth axis ( $s-p_z$ ) in quantum dots (QDs) [14], transitions that are only allowed for TM-polarized light. Thanks to the large conduction band offset in the GaN/AlN system (:1.8 eV [15]), the intraband energy difference can be tuned to 1.55  $\mu\text{m}$  by controlling the size and composition of the nanostructures. Furthermore, the strong electron-phonon interaction in these materials leads to intraband relaxation times in the range of 150–400 fs [16–21] at telecom wavelengths, confirming their potential for ultrafast all-optical devices. On the other hand, nonlinearities are enhanced by quantum confinement in nanostructures, as already demonstrated by second-harmonic generation in GaN/AlN QWs [22], and measurements of the high third-order nonlinear susceptibility in GaN/AlN QWs [16] and QDs [21]. Thus, the onset of nonlinear interactions is expected at lower power levels than in bulk materials.

The use of intraband transitions in GaN/AlGaIn QWs for the implementation of all-optical modulators at telecommunication wavelengths was first proposed by Suzuki *et al.* [18,23]. Since then, all-optical switching at  $\sim 1.55$   $\mu\text{m}$  with sub-picosecond response time has been demonstrated by several groups. In general, these devices consist of GaN/AlN MQWs embedded in a ridge WG. Control switching energies as low as 38 pJ for 10 dB modulation depth [24] and 25 pJ for 5 dB contrast [25] have been reported using a WG with an AlN cladding below the active GaN/AlN QWs, and GaN or  $\text{Si}_x\text{N}_y$  as the upper cladding layer, respectively.

Comparative studies using the forward degenerate four-wave mixing technique in a boxcar configuration point to an increase of  $\chi^{(3)}$  by a factor of five in GaN/AlN QDs compared to GaN/AlN QWs [21]. Furthermore, the  $s-p_z$  intraband absorption saturation of GaN/AlN QDs is achieved for a saturation intensity  $< 1.4$   $\text{W}/\mu\text{m}^2$  ( $< 0.27$   $\text{pJ}/\mu\text{m}^2$ ) [26], significantly smaller than the value reported for GaN/AlN QWs (9.46  $\text{W}/\mu\text{m}^2$  [24]).

In this work we report the fabrication of III-nitride WGs for nonlinear-optical switching at 1.55  $\mu\text{m}$  using intraband transitions in GaN/AlN QWs and QDs. Linear transmittance measurements are used to estimate the WGs coupling and propagation losses. Nonlinear optical absorption measurements are carried out in order to study the transmittance modulation capabilities of QW- and QD-based WGs. A transmittance increase of 10 dB for 8 pJ and 150 fs pulses is achieved in 2- $\mu\text{m}$ -wide QD-based WGs.

## 2. Optical and electrical design

The electrical design of the active region was carried out taking into account both optical and electrical considerations. The optical design was investigated using the RSoft BeamProp finite-difference beam-propagation mode solver. The optical modes propagated through the WG were calculated at  $\lambda_0 = 1.55$   $\mu\text{m}$  assuming 1.746, 2.120 and 2.317 as the linear refractive indices for sapphire, AlN and GaN, respectively. The electronic properties of the GaN/AlN heterostructure were modeled using the Nextnano<sup>3</sup> 8-band k.p Schrödinger-Poisson solver [27] with the material parameters described in ref [28].

The two samples under consideration consist of 3 layers of GaN/AlN QDs or QWs embedded in a guiding structure based on a 600-nm-thick GaN layer deposited on a 1.1- $\mu\text{m}$ -thick AlN-on-sapphire template, as shown in Fig. 1(a). The choice of AlN as a substrate is due to the smaller in-plane lattice constant in comparison with GaN, which keeps the structure under compressive strain and hence prevents the formation of cracks in the active region. Furthermore, the smaller refractive index of AlN in comparison to GaN pushes the optical modes towards the GaN layer, keeping them away from the highly-dislocated sapphire/nitride interface.

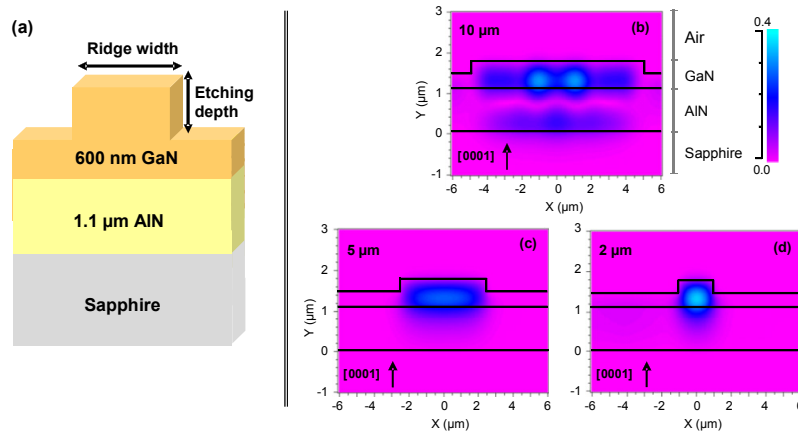


Fig. 1. (a) Schematic description of the GaN/AlN WG device. (b-d) Cross-section and normalized modal amplitude color maps for GaN/AlN WGs with different ridge widths: 10, 5 and 2  $\mu\text{m}$ , respectively.

The GaN layer thickness was chosen so as to achieve single mode guiding for ridge widths affordable with optical lithography ( $\sim 2 \mu\text{m}$ ). A set of simulations varying the ridge width (from 2 to 50  $\mu\text{m}$ ) and the etching depth (from 50 to 600 nm) was performed. From the simulations presented in Figs. 1(b)–1(d), 2- $\mu\text{m}$ -wide WGs are considered single mode while WGs with widths of 5  $\mu\text{m}$  lead to quasi-single mode propagation for WG lengths in the range of 1-2 mm. Strong multimode propagation is obtained when increasing the WG width above 5  $\mu\text{m}$ . At the same time, the etching depth from 250 to 550 nm has no relevant impact on the output modal profile, presenting in all cases a reduced slab modal guiding. Figure 2 (left) illustrates the normalized output modal profile for a 2- $\mu\text{m}$ -wide WG with different values of etching depth: 100, 200 and 350 nm. An etching depth of 350 nm is selected for the fabrication of the WGs since it provides the lowest modal effective area in the range under study, as shown in Fig. 2 (middle). For these dimensions (2–5  $\mu\text{m}$  wide and 350 nm deep ridge), the optical power lost at the AlN/sapphire interface is  $\sim 1\%$  of the total power. The simulations also reveal the difference in light confinement between the 5- $\mu\text{m}$ - and the 2- $\mu\text{m}$ -wide WGs. An increase of  $\sim 20\%$  of the output peak amplitude is estimated for 2- $\mu\text{m}$ -wide WGs with respect to 5- $\mu\text{m}$ -wide WGs [see Fig. 2 (right)]. For similar coupling losses, the 2- $\mu\text{m}$ -wide WG should therefore exhibit lower saturation input power.

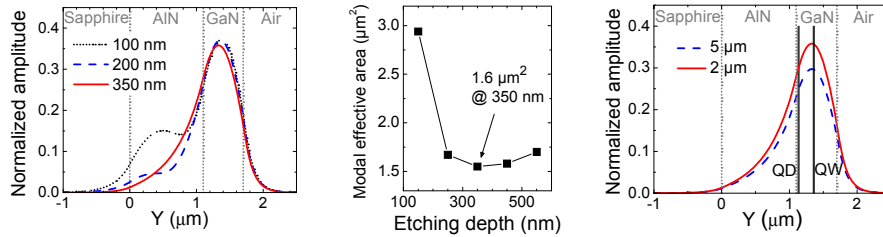


Fig. 2. (left) Normalized output modal amplitude profile for a 2- $\mu\text{m}$ -wide WG with different ridge etching depths: 100, 200 and 350 nm. (middle) Estimated modal effective area as a function of the ridge etching depth for the 2- $\mu\text{m}$ -wide WG. (right) Normalized output modal amplitude profile for both 5- $\mu\text{m}$ - and 2- $\mu\text{m}$ -wide WGs with 350-nm-deep ridges. The location of QD/QW layers in the experimental structures is indicated by the black vertical lines.

The active media was limited to only 3 periods of GaN/AlN QWs/QDs in order to grant a measurable transmission in 2-mm-long WGs. The dimensions of the active nanostructures, namely Si-doped 1.5 nm GaN (6 ML) / 3 nm AlN QWs, or  $\sim 1$  nm high ( $\sim 4$  ML) Si-doped GaN QDs separated by 3 nm AlN barriers, are defined so as to tune the intraband absorption to  $1.55 \mu\text{m}$ , in agreement with previous results [28,29] (see conduction band profile in the inset of Fig. 3). Regarding the location of the active nanostructures within the guiding GaN layer, in the case of QWs, they are placed at the modal amplitude maximum, *i.e.* 250 nm above the AlN template/GaN interface. In the case of QDs, a certain compressive strain is required to activate the three-dimensional growth. Thus, the best choice from the epitaxial viewpoint would be their deposition directly on the AlN template, profiting from the 2.5% lattice mismatch between GaN and AlN. This location would imply a decrease of the modal overlap with the active layer of  $\sim 22\%$  [see Fig. 2 (right)], which could be compensated if needed by increasing the number of QD periods. However, theoretical calculations of the electronic profile show that the difference of spontaneous and piezoelectric polarization between GaN and AlN leads to a total depletion of the QDs, as illustrated in Fig. 3 (dot-dashed line). Therefore, a GaN buffer layer of  $\sim 25$  nm is deposited prior to the growth of the QDs, thick enough to obtain flat-band conditions in the QDs (see Fig. 3, solid line), while keeping enough elastic energy to induce the QD formation.

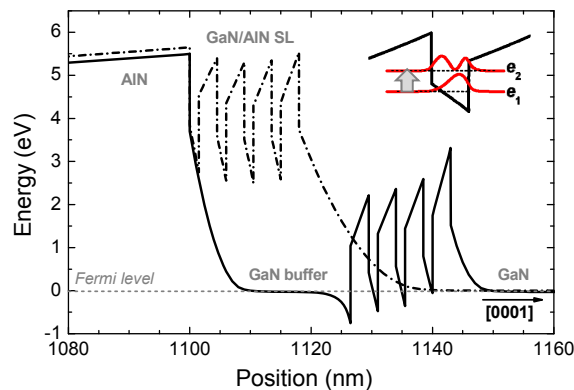


Fig. 3. Conduction band profile of the active GaN/AlN superlattice considering the whole WG structure. Inset: Conduction band profile of one of the GaN/AlN QWs designed to obtain a resonant intraband transition at  $\sim 1.55 \mu\text{m}$ .

### 3. Structure growth and waveguide fabrication

The samples were synthesized by plasma-assisted molecular-beam epitaxy using 1.1- $\mu\text{m}$ -thick AlN-on-sapphire substrates. The growth rate was  $\sim 280$  nm/h and the growth temperature was

720°C, low enough to ensure a negligible GaN decomposition and to prevent a thickness reduction of the GaN nanostructures during AlN capping process ( $\leq 730^\circ\text{C}$ ) [30]. The QW-containing structure was deposited under Ga-rich conditions, without growth interruptions. In the case of the QD-based structure, the AlN barriers were synthesized under Al-rich conditions, followed by nitrogen exposure to consume the Al excess. Then, the GaN QDs are formed by deposition of 3 monolayers of GaN under N-rich conditions (N/Ga flux ratio = 0.8), followed by a 15 s growth interruption in vacuum. These growth conditions result in a high density ( $10^{11}$ – $10^{12}$  cm $^{-2}$ ) of small QDs (1–1.5 nm high) connected to the underlying AlN by a 2 ML thick defect-free GaN wetting layer [29]. The dots are subsequently capped with 3 nm of AlN, which rapidly recovers a planar surface. Both QWs and QDs were Si doped ([Si]  $\sim 10^{20}$  cm $^{-3}$ ) in order to populate the first confined electronic level and enable efficient intraband absorption.

For both QW- and QD-based samples, the top GaN surface present a flat morphology with atomic terraces and a root-mean-squared (rms) surface roughness of  $\sim 1.0$  nm, measured by atomic force microscopy in an area of  $5 \times 5$   $\mu\text{m}^2$ . The active regions were studied by high-resolution transmission electron microscopy (HRTEM), as illustrated in Figs. 4(a) and 4(b). The images show the different morphology of QW and QD layers, both displaying chemically sharp GaN/AlN interfaces at the atomic scale. The QDs present a height of  $\sim 1$  nm and a base diameter of  $\sim 7$  nm.

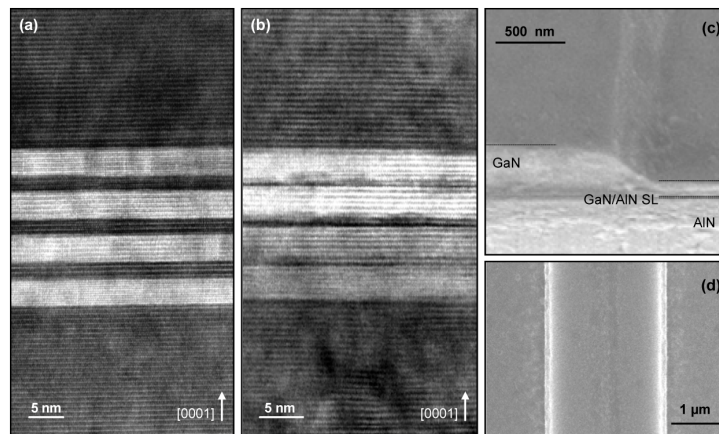


Fig. 4. HRTEM images of the active region of the samples containing 3 layers of (a) Si-doped GaN/AlN QWs and (b) Si-doped GaN/AlN QDs. (c) 45° tilted FESEM image of the facet, and (d) plane view of a fabricated 2- $\mu\text{m}$ -wide GaN/AlN QD-based WG.

The WGs were defined by optical lithography with widths of 2 and 5  $\mu\text{m}$ . The 350-nm-deep ridge was patterned by induced coupled plasma reactive-ion etching (ICP-RIE) using  $\text{SiCl}_4$  and  $\text{N}_2$  plasma at room temperature. The WGs were cut using an automated dicing saw. After dicing, the samples were mechanically polished to obtain mirror-like facets. Figures 4(c) and 4(d) show the field emission scanning electron microscopy (FESEM) images of a 2- $\mu\text{m}$ -wide GaN/AlN WG.

#### 4. Optical measurements

Three sets of WGs were measured: 5- $\mu\text{m}$ -wide QW-based WG, and 5- $\mu\text{m}$ -wide and 2- $\mu\text{m}$ -wide QD-based WG (S1, S2, and S3 in Table 1, respectively). The propagation of both TE- and TM-polarizations of light was experimentally examined in the linear and nonlinear optical regimes using a mode-locked fiber laser operating at 1.55  $\mu\text{m}$  with a pulse width of 100 fs and a repetition rate of 100 MHz. The light at the output of the laser was coupled into an optical fiber and split using an optical fiber coupler (99/1); *i.e.* 99% of the signal is used to perform



the linear and nonlinear measurements and the rest is used as a reference. Light with a controlled TM or TE polarization is coupled into the WG by means of a  $\sim 2.5\text{-}\mu\text{m}$ -diameter-spot lensed fiber. At the input of the WG, the pulse is broadened by the whole optical system up to 150 fs. The WG is mounted on a 3-axis positioning stage with tilt and rotation controls. The collection of light at the output of the WG is performed with a microscope objective lens and an infrared camera to monitor the optical mode, or with a single mode fiber to measure the output optical power. Figures 5(a) and 5(b) illustrate the near-field images of transmitted light in the linear regime through 5- $\mu\text{m}$ - and 2- $\mu\text{m}$ -wide WGs, respectively.

**Table 1. Summary of the structural parameters and experimental results obtained for the three samples under study (S1, S2 and S3).**

Sample #	Active nanostructures	Ridge width ( $\mu\text{m}$ )	Energy for 3 dB TM contrast (pJ)	Energy for 10 dB TM contrast (pJ)
S1	QWs	5	8	24
S2	QDs	5	5	13
S3	QDs	2	3	8

Both propagation and coupling losses were estimated through the cutback method [31], measuring the transmittance of TE- and TM-polarized light through similar WGs with different lengths, under low incident power conditions ( $-12\text{ dBm}$ , well below the absorption saturation level). It has to be pointed out that the different lengths of the WGs have been obtained by polishing the output facet with a slight angle ( $\sim 3^\circ$ ). Thus, for all the WGs under study, coupling losses obtained through the cut-back method are expected to be overestimated. As an example of the cut-back method, Fig. 5(c) shows the variation of the transmittance as a function of the WG length for sample S1. From those data, we extract propagation losses in the range of  $\sim 28\text{ dB/mm}$  for TM-polarized light, including saturable and non-saturable losses. The 2 dB difference between TM and TE coupling losses is likely due to the asymmetry of the WG geometry. In the following transmittance measurements performed in isolated optical WGs, we have considered that the measured coupling losses are equally distributed between both facets.

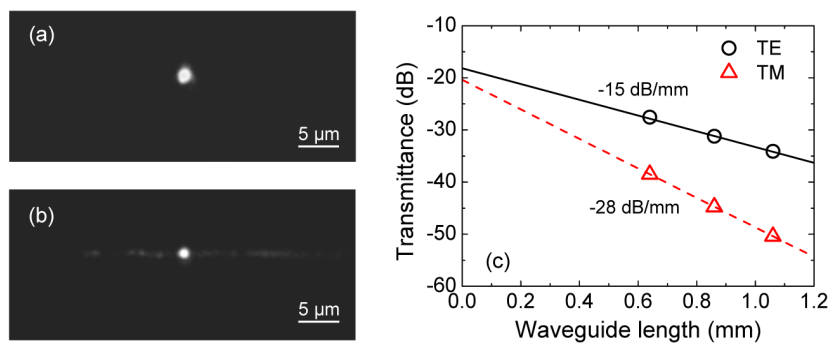


Fig. 5. Near-field image of transmitted light through (a) 5- $\mu\text{m}$ -wide and (b) 2- $\mu\text{m}$ -wide QD-based WGs. (c) Cutback method: Experimental TE-TM transmittance at minimum incident power ( $-12\text{ dBm}$ ) as a function of the WG length for the 5- $\mu\text{m}$ -wide QW-based WG. The experimental points correspond to the average of transmittance measurements in 3 WGs for each WG length.

Figure 6(a) illustrates transmittance measurements for TE- and TM-polarized light as a function of the incident optical power for a 1-mm-long S1 WG. The transmittance of TE-polarized light is constant for the analyzed power range. In contrast, the transmitted TM-polarized light increases with the incident optical power due to the saturation of the  $e_1$ - $e_2$  intraband absorption in the QWs. A 10 dB change in the TM transmittance is achieved for input pulse energies of  $\sim 24\text{ pJ}$  [see Fig. 6(b)], lower than the 38 pJ reported by Li *et al.*

[24,32,33] in a similar WG structure (600 nm GaN on AlN, 1-mm-long WG and 3- $\mu$ m-wide ridge) but incorporating 30 GaN/AlN QWs. In this latter structure, the QWs were inserted between the AlN and the GaN layers. Our achievement of similar results with only 3 QWs could be explained by the partial carrier depletion of the 30-QW structure due to piezoelectric and spontaneous polarization, as described in Fig. 3. Thus, only a few of the 30 QWs would participate to the intraband absorption.

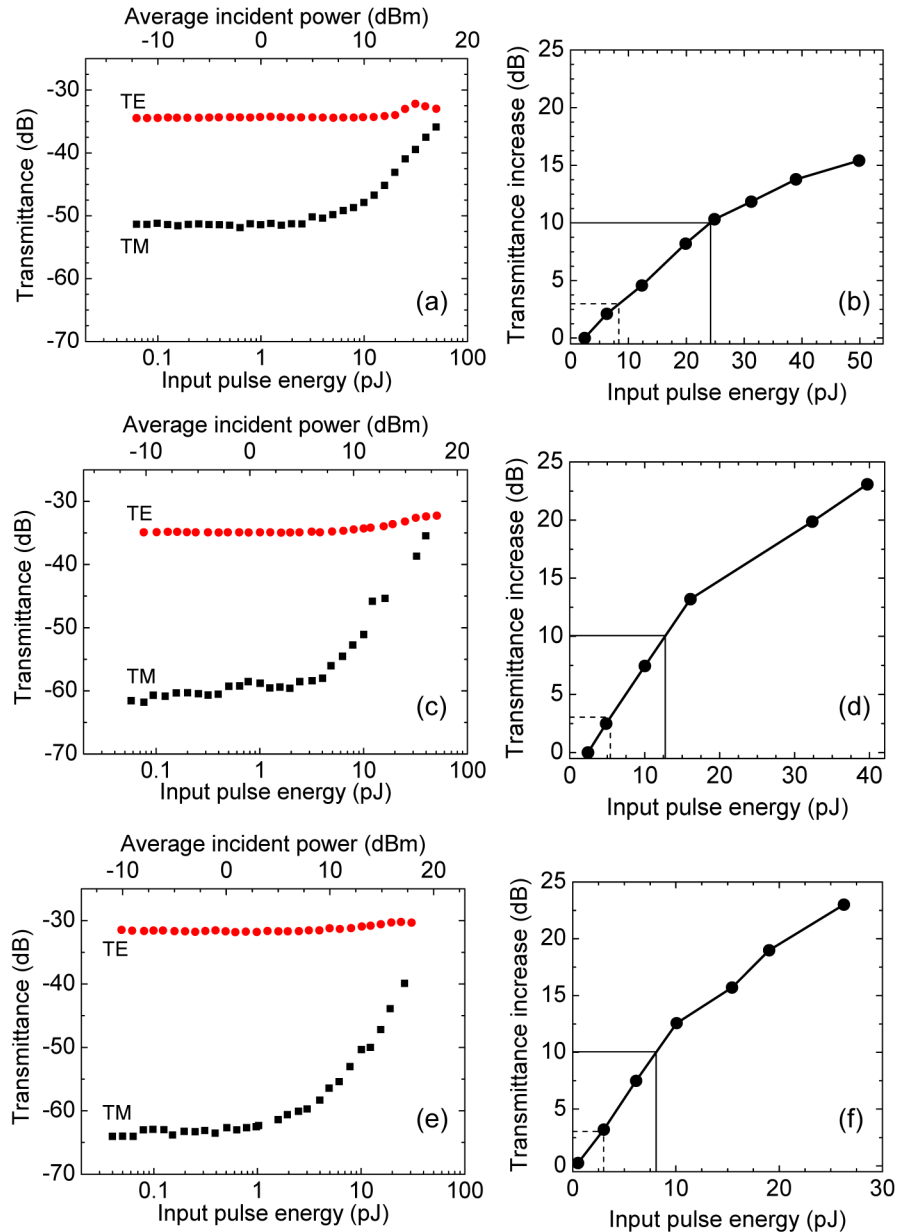


Fig. 6. Transmittance for TE- and TM-polarized light (left) and transmittance increase versus control pulse energy for TM-polarized light measured (right) in (a,b) a 1-mm-long 5- $\mu$ m-wide QW-based WG (S1), (c,d) a 1.5-mm-long 5- $\mu$ m-wide QD-based WG (S2), and (e,f) a 1.5-mm-long 2- $\mu$ m-wide QD-based WG (S3).



Figures 6(c) and 6(d) depict the optical TE and TM transmittance and the transmittance increase for TM-polarized light, respectively, as a function of the input pulse energy for a 5- $\mu\text{m}$ -wide QD-based WG (S2) with a length of 1.5 mm. In this case, input pulse energies of  $\sim 13$  pJ are required to obtain a 10 dB change in the TM light transmittance, assuming similar coupling losses as those estimated for both 5- $\mu\text{m}$ -wide QW- and QD-based WGs. The improvement obtained in comparison to the QW structure might be explained by the three dimensional confinement in the QDs, which prevents lateral escape of carriers, thus favoring absorption saturation.

The modulation of the transmittance for TM-polarized light can be further enhanced by reducing the WG ridge to 2  $\mu\text{m}$  to obtain single mode propagation, as illustrated in Figs. 6(e) and 6(f). In this case, the input pulse energy required for 10 dB absorption saturation is as low as  $\sim 8$  pJ with 150 fs pulses.

## 5. Conclusions

The suitability of intraband transitions in GaN/AlN nanostructures for application in all-optical switching at 1.55  $\mu\text{m}$  has been demonstrated by nonlinear optical absorption measurements carried out in GaN-on-AlN WGs containing 3 periods of GaN/AlN QWs or QDs. In the case of 5- $\mu\text{m}$ -wide QW-based WGs, the transmitted TM-polarized light increases with the incident optical power due to the saturation of the  $e_1$ - $e_2$  intraband absorption in the QWs. A 10 dB change in the transmittance of TM-polarized light is achieved for input pulse energies of  $\sim 24$  pJ with 150 fs pulses. This value is improved by almost a factor of 2 by the replacement of QWs by QDs as active media, thanks to their three-dimensional carrier confinement. The reduction of the WG width to 2  $\mu\text{m}$  results in a further decrease of the required input pulse energy to  $\sim 8$  pJ for 10-dB-modulation, taking advantage of the single mode propagation along the WG.

## Acknowledgments

This work was supported by Spanish Government Project TEC2012-37958-C02-01, Comunidad de Madrid Project S2009/ESP-178, and the EU Marie Curie IEF ‘SolarIn’ (#331745), and EU ERC-StG ‘TeraGaN’ (#278428) projects.